Impact of the glass transition on exciton dynamics in polymer thin films

Philipp Ehrenreich,[1] Daniel Proepper,[2] Alexander Graf,[1] Stefan Jores,[1] Alexander V. Boris,[2] and Lukas Schmidt-Mende[1,*]
[1]*Department of Physics, University of Konstanz, P.O. Box 680, 78457 Konstanz, Germany*
[2]*Max-Planck-Institut für Festkörperforschung, Heisenbergstraße 1, 70569 Stuttgart, Germany*
(Received 26 April 2017; revised manuscript received 13 September 2017; published 9 November 2017)

In the development of organic electronics, unlimited design possibilities of conjugated polymers offer a wide variety of mechanical and electronic properties. Thereby, it is crucially important to reveal universal physical characteristics that allow efficient and forward developments of new chemical compounds. In particular for organic solar cells, a deeper understanding of exciton dynamics in polymer films can help to improve the charge generation process further. For this purpose, poly(3-hexylthiophene) (P3HT) is commonly used as a model system, although exciton decay kinetics have found different interpretations. Using temperature-dependent time-resolved photoluminescence spectroscopy in combination with low-temperature spectroscopic ellipsometry, we can show that P3HT is indeed a model system in which excitons follow a simple diffusion/hopping model. Based on our results we can exclude the relevance of hot-exciton emission as well as a dynamic torsional relaxation upon photoexcitation on a ps time scale. Instead, we depict the glass transition temperature of polymers to strongly affect exciton dynamics.

DOI: 10.1103/PhysRevB.96.195204

I. INTRODUCTION

Conjugated polymers promise to be an attractive material class for future electronic applications because of their printability [1], mechanical flexibility [2,3], and inexhaustible material occurrence. For application in organic solar cells it is additionally important to bring power conversion efficiencies to a competitive level [4]. This goal can be achieved by a maximization of the external quantum efficiency, i.e., the product of light absorption efficiency, exciton diffusion efficiency, exciton separation efficiency, and charge collection efficiency. Common characteristics of polymers like a low electric permittivity and structural disorder in thin films usually cause a very strong electronic localization with limited exciton diffusion lengths smaller than 20 nm [5]. Exciton diffusion is typically described within the framework of Förster resonance energy transfer (FRET) and is strongly affected by orientational as well as energetic disorder [5]. Material anisotropy [6], structural, and in particular energetic disorder give rise to a broad density of states (DOS) with enhanced trapping probability and recombination rates of excitons [7,8]. Processing techniques [9], variations in molecular weight [10], or defects along the backbone limit the fabrication of highly crystalline polymer films with a narrow energetic site distribution. It is the variety of such influences which necessitates model systems that allow for a systematic investigation of their individual impact on exciton dynamics. A polymer well understood with respect to structure-related properties is poly(3-hexylthiophene) (P3HT) [11–13]. Furthermore, its homopolymeric nature makes P3HT an attractive candidate for such investigations while no additional multipole moments and complicated chemical modifications have to be accounted for [14,15].

In fact, P3HT has already been subject to many investigations on excitons in conjugated polymers, although seemingly conflicting findings have put its model system character into question. Banerji *et al.* [16] could observe ultrafast exciton formation with radiative decay dynamics starting already on a sub-200-fs time scale. It is shown that early time spectra exhibit significant differences from later time scales, namely a strongly enhanced 0-0 transition and an emission feature below 600 nm, i.e., at energies larger than the absorption onset. These two observations have occurred in various studies, although their interpretation varies [16–19]. Different dynamics of the 0-0 transition compared to higher vibronic transitions have been explained by the emission from not yet relaxed excitons to H-aggregates [16] as well as torsional relaxation of the polymer backbone after excited-state formation [17], while there are also reports that do not even observe such dynamic differences of vibronic replicas [18]. Also, the occurrence of a high-energy emission peak has found different explanations in the literature. It has been suggested that this additional peak arises from disordered polymer segments [16], but it has been also attributed to hot-exciton emission prior to exciton relaxation [19]. Overall, a dynamic redshift is seen in all emission spectra of P3HT which is commonly explained by exciton migration to lower energetic sites in the DOS. However, also here an alternative explanation is offered which attributes this redshift to the influence of an evolving electric field from photogenerated charge carriers in the polymer film [18].

Such diverse conclusions and apparently contradictory observations challenge P3HT to be a suitable model system for general investigations on the fundamental concept of exciton migration in polymer thin films. Instead, it is necessary to ask whether conclusions and findings on P3HT are comparable and valid for other systems. By means of steady-state and time-resolved photoluminescence (PL) spectroscopy in a temperature range from 5–370 K, we show that P3HT follows the same exciton diffusion/hopping model as other organic semiconductors [20,21] if individual material properties like the glass transition temperature T_g are taken into account [5,7,22]. We show compelling evidence that amorphous and aggregated polymer domains are electronically decoupled at T_g, which results in a high-energy emission peak in PL spectra.

*Corresponding author: lukas.schmidt-mende@uni-konstanz.de

Conclusions on structural changes with temperature are supported by temperature-dependent spectroscopic ellipsometry.

II. EXPERIMENTAL METHODS

For spectroscopic ellipsometry, we have used P3HT thin films on $10 \times 10\,\mathrm{mm}^2$ Si substrates with a natural SiO_2 surface of 2 nm. Before spin-coating the polymer from solution, substrates were cleaned in an ultrasonic bath subsequently in acetone and isopropanol for 10 min. After drying the samples in a N_2 gas stream, we have further cleaned them in an oxygen plasma for 7 min. In a next step regioregular poly(3-hexylthiophene) (rrP3HT, Rieke Metals, $M_W = 51$ kDa, PDI $= 2.1$, $>96\%$ regioregularity) or regiorandom poly(3-hexylthiophene) (rraP3HT, Rieke Metals, $M_W = 51$ kDa, $<81\%$ regioregularity) is spin-coated from a chlorobenzene solution with a concentration of 10 mg/ml to produce 50 nm films and 20 mg/ml for 100 nm films. All samples are processed in air and measured without further treatment. For photoluminescence measurements substrates were replaced by SiO_2 while the fabrication procedure is identical.

Steady-state photoluminescence measurements have been collected with a home-built spectrometer. It consists of a solid-state diode laser as excitation source and a LOT MSH-300 monochromator equipped with a Hamamatsu S2386-5K Si-diode detector. The excitation beam is modulated at a frequency of 170 Hz and the signal is evaluated with a Zurich HF2LI lock-in amplifier. Calibration with respect to intensity was done with a spectral fluorescence standard kit certified by BAM (Sigma-Aldrich). The same calibration standard has been applied on the Hamamatsu C10910-01 streak camera setup, which we used for time-resolved photoluminescence spectroscopy. In order to account for field inhomogeneities within the deflection plates of the streak camera a shading correction was performed. For this purpose, we have illuminated a Spectralon plate with a tungsten lamp. Diffusely scattered light by the plate is collected in the focal plane of the collecting lens optics in front of the spectrograph. For excitation, laser pulses ($t_p < 120$ fs) from a Ti:sapphire oscillator (Coherent Mira-HP) were used at a repetition rate of 76 MHz. By means of second-harmonic generation (HarmoniXX, APE) or frequency conversion in an optical parametric oscillator (Mira OPO, APE), samples are excited at 400 or 530 nm. Depending on the chosen time range (TR), the time resolution was as good as 2.5 ps (TR2) and 28 ps (TR5). The fluence was held below 1 nJ/cm² in order to avoid nonlinear exciton dynamics. All PL measurements have been performed in a continuous-flow cryostat (Janis ST100) in evacuated atmosphere ($p < 10^{-5}$ mbar). For decay analysis, we have deconvoluted our spectra with the instrument response function (IRF). The spectroscopic ellipsometry data were taken on a J.A. Woollam Co. variable angle spectroscopic ellipsometer (VASE) system equipped with a home-built UHV cold-finger cryostat with a base pressure of 10^{-10} mbar. The spectroscopic angles Ψ and Δ were fitted by a three-layer model of a Si substrate, SiO_2 interlayer with a thickness of 2 nm, and a polymer thin film. Si and SiO_2 were modeled by literature data. The thickness of SiO_2 was determined experimentally from measurements on a bare Si substrate. At each temperature the polymer film thickness was determined by fitting a Cauchy model to the spectral range between 1.2 and 1.8 eV well below the absorption edge, i.e., $k = 0$ in this range. With the film thickness fixed, the effective complex refractive index $\tilde{n} = n + ik$ was fitted in the energy range from 2.5 to 3.2 eV in a point-by-point fashion, while the absorption of aggregated rrP3HT is modeled with a series of three Tauc-Lorentz oscillators.

III. RESULTS

A. Steady-state PL spectra

In this study we have investigated the fluorescence behavior of 50 nm P3HT films depending on excitation energy and temperature. Room-temperature steady-state PL spectra of rrP3HT are shown in Fig. 1. Below the optical energy gap of about 2 eV, emission spectra are independent of excitation energy. However, when we excite mainly amorphous polymer domains at 405 nm we observe an additional and relatively broad peak at energies larger than 2 eV. Interestingly, this transition is only present around room temperature and does not occur if we excite with 532 nm (see Supplemental Material, Fig. S1 [23]).

For 532 nm excitation we observe that the PL intensity of rrP3HT is continuously decreasing with increasing temperature until it saturates at 250 K. In contrast, when exciting with 405 nm we observe a small local maximum at 300 K and the PL intensity is further increasing for even higher temperatures

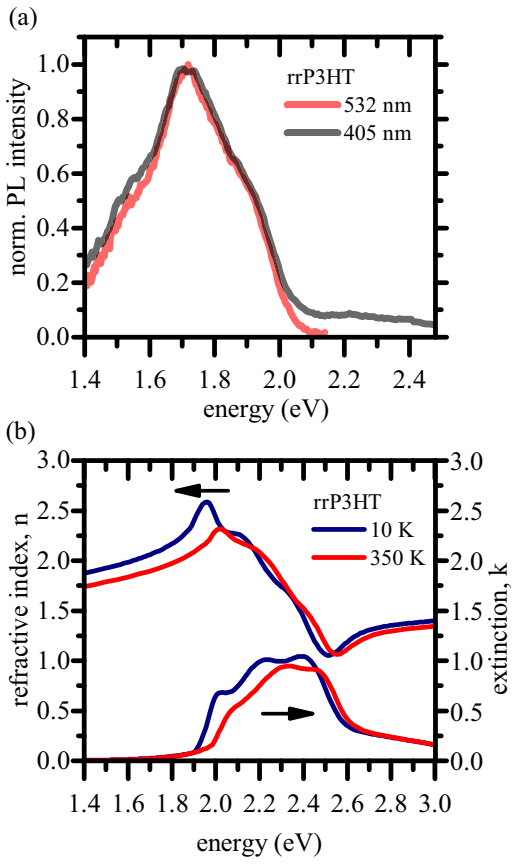

FIG. 1. (a) Normalized steady-state PL spectra of rrP3HT. (b) Refractive index n and extinction k of rrP3HT at 10 and 350 K, respectively.

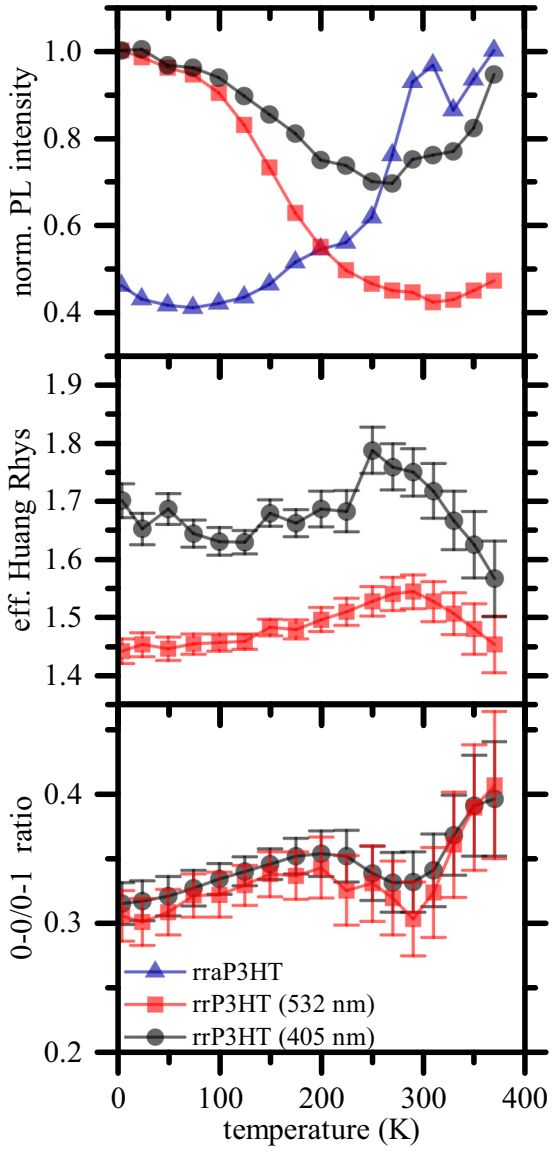

FIG. 2. Top: Peak PL intensity as a function of temperature, normalized to the maximum emission spectrum. rraP3HT films were excited at 405 nm. Middle: effective Huang-Rhys factor extracted from fits with Eq. (1) on steady-state spectra of rrP3HT. Bottom: 0-0/0-1 transition ratio extracted from fits with Eq. (1) on steady-state PL spectra of rrP3HT; lines are a guide for the eye and error bars represent the standard deviation obtained from fits.

(Fig. 2). This is in agreement with rraP3HT, for which we detect a strong increase in PL intensity above 250 K with a local maximum just below 300 K. In order to investigate these observations with respect to molecular configuration and microstructure, we have modeled temperature-dependent PL spectra within the Franck-Condon (FC) picture. Different from single-molecule emission, dipole coupling influences both the transition probability, which usually just follows a Poisson distribution, and inhomogeneous line broadening due to energetic disorder. P3HT is a conjugated polymer with significant torsional disorder along the backbone. In addition, the size of aggregates is randomly distributed in an amorphous matrix. Consequently, transition lines are well described with Gaussian functions Γ. Dipole coupling, on the other hand, depends also on the dimensions of aggregates, i.e., transition dipole moments of neighboring chromophores. The length scale of each delocalized π-orbital system along the backbone determines the strength of intramolecular coupling while intermolecular coupling occurs in the π-orbital stacking direction [11]. J-aggregates are dominated by intramolecular coupling forces, whereas H-aggregates are characterized by a strong intermolecular interaction in the π-stacking direction. In H-aggregates, the oscillator strength for the 0-0 transition is zero [24]. Disorder can break symmetry and allows for 0-0 transitions to a certain degree. For this reason, Clark *et al.* [24] suggest PL modeling within a modified FC model in which the 0-0 transition is treated individually:

$$I(\omega) \propto (\hbar\omega)^3 n^3 e^{-\lambda_{\mathrm{eff}}^2} \times \left[\alpha\Gamma(\hbar\omega - E_0) + \sum_{m=1}^{j} \frac{\left(\lambda_{\mathrm{eff}}^2\right)^m}{m!}\Gamma(\hbar\omega - E_0 - mE_p)\right] \quad (1)$$

n is the refractive index, λ_{eff}^2 is the effective Huang-Rhys factor, m is the vibrational mode number, E_0 is the energetic position of the 0-0 transition, E_p is the energy of a C=C stretching mode, and α is the amplitude describing the 0-0 transition. In general, all of these parameters are temperature dependent, a fact which has often been ignored in the past. We have determined the evolution of the refractive index $n(\omega,T)$ and extinction coefficient $k(\omega,T)$ by means of temperature-dependent ellipsometry. In Fig. 1(b) two measurements at 10 and 350 K are shown (for more details see Supplemental Material, Figs. S4–S8 [23]). PL spectra of rrP3HT are modeled with Eq. (1) by using $n(\omega,T)$, which reveals a rather constant λ_{eff}^2 up to 225 K with an increasing 0-0/0-1 transition ratio independent on the excitation energy (Fig. 2). This observation can be explained by thermally activated emission from the 0-0 transition while a constant λ_{eff}^2 suggests aggregates to be in a constant phase. Above 225 K, λ_{eff}^2 increases to a local maximum and the 0-0/0-1 transition ratio decreases to a local minimum. For temperatures higher than 300 K, λ_{eff}^2 decreases continuously and the 0-0 transition is enhanced. It is worth noting that λ_{eff}^2 is significantly lower if the sample is excited at 405 nm. This can be rationalized by the fact that morphologically more amorphous polymer domains are excited (Fig. 2).

In order to resolve the dynamic evolution of exciton emission, it is necessary to have a closer look at time-resolved spectra.

B. PL dynamics

In Fig. 3(a) we show time-resolved PL streak camera images of rrP3HT for three selected temperatures, i.e., 77, 250, and 350 K. As demonstrated in the Supplemental Material [23], they represent universal observations below 200 K (low-temperature regime), between 200 and 300 K (intermediate-temperature regime), and above 300 K (high-temperature regime). For all cases, there is a kinetic spectral redshift, a significantly reduced exciton lifetime with increasing temperature, and a high-energy emission peak at 250 K. Exciton

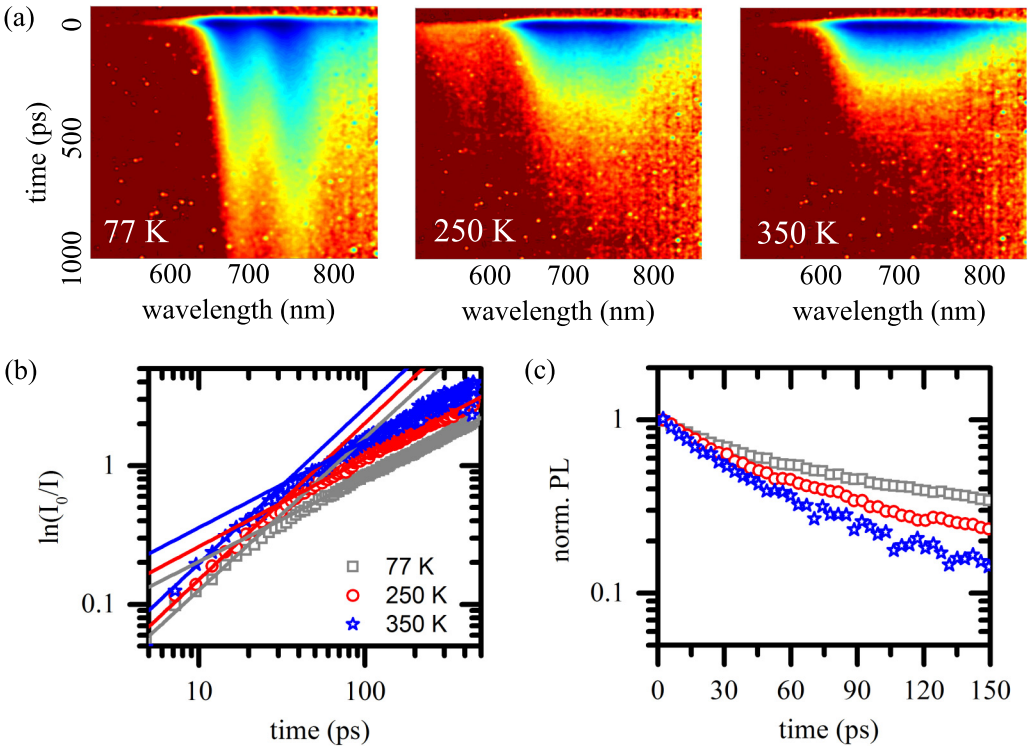

FIG. 3. (a) Time-resolved PL of rrP3HT measured at 77, 250, and 350 K using an excitation wavelength of 405 nm. (b) $\ln(I_0/I)$ decay dynamics of the 0-1 transition extracted from streak images. Solid lines represent stretched exponential fits using Eq. (2). The initial decay is characterized by a simple exponential ($\beta = 1$), while for longer times β converges to 0.5. (c) PL decay of the 0-1 transition on a semilogarithmic scale.

transfer in conjugated polymers has often been described by dipole coupling to neighboring energetic sites following an incoherent diffusive random walk [20,21]. Bässler and co-workers have used the Kohlrausch-Williams-Watts (KWW) function to describe the exciton migration process toward energetically lower-lying states in a broad DOS, for which the number of energetically favorable neighbors is dynamically reducing:

$$I(t) = I_0 \exp[-(t/t_0)^{\beta}]. \quad (2)$$

Diffusive exciton migration is characterized by a single-exponential decay of lifetime t_0 ($\beta = 1$). If, however, tail states in the DOS are reached, excitons can only be transferred via direct single-step FRET. This is characterized by $\beta = 0.5$ [20]. As presented in Fig. 3(b), also our data are well described within the KWW description. For short times ($\ll$100 ps) the exciton decay rate is time independent and can be characterized by a single exponential, while decay kinetics gradually turn into a $\beta = 0.5$ description of longer times. We have summarized fit results within the two asymptotic regimes in Table 1. Deviation from theoretical values occurs due to a gradual and broad crossover region in between the two regimes, as it is better seen from plots using a linear time axis [Fig. 3(c)]. Consequently, fit results slightly depend on chosen fit ranges although qualitative observations are not affected.

Another signature for energetic relaxation in a broad DOS is a dynamic spectral redshift in combination with a time-dependent 0-0/0-1 transition ratio. In Fig. 4(a) we show normalized spectral cuts of our streak camera images. At 77 K, we observe a redshift of approximately 60 meV in combination with a progressive reduction of the 0-0 transition relative to higher vibronic replica. In total the 0-0/0-1 transition ratio decreases by more than 40%, while over 30% fall upon the first 200 ps [Fig. 4(b)]. In an intermediate temperature regime (represented by 250 K), the 0-0 transition is reduced by only 20% from the initial amplitude and for 350 K the 0-0/0-1 ratio decreases even less pronounced with time. At 250 K, the redshift takes place within the first 100 ps, while stable conditions are reached in less than 50 ps for 350 K. In both cases there is no significant impact on spectra for longer times than 200 ps. Thermal broadening, strong peak overlap, and a reduced signal-to-noise ratio lead, however, to fit inaccuracies as seen in a relatively large data scattering in Figs. 4(b) and 4(c) for higher temperatures and later times.

Although these observations evoke the appearance of different excitonic dynamics for vibronic replicas, the 0-0 transition is reduced because of a progressive change in morphology and energetic order. Seemingly different kinetics of the 0-0

TABLE I. β obtained from fits temperature using Eq. (2) on PL decays presented in Fig. 3 for short times ($\beta_s \ll 100$ ps) and longer times ($\beta_l > 100$ ps). Fit uncertainties are in parentheses.

Temperature (K)	β_s	β_l
77	1.10 (±0.04)	0.60 (±0.01)
250	1.13 (±0.05)	0.63 (±0.01)
350	1.12 (±0.05)	0.62 (±0.02)

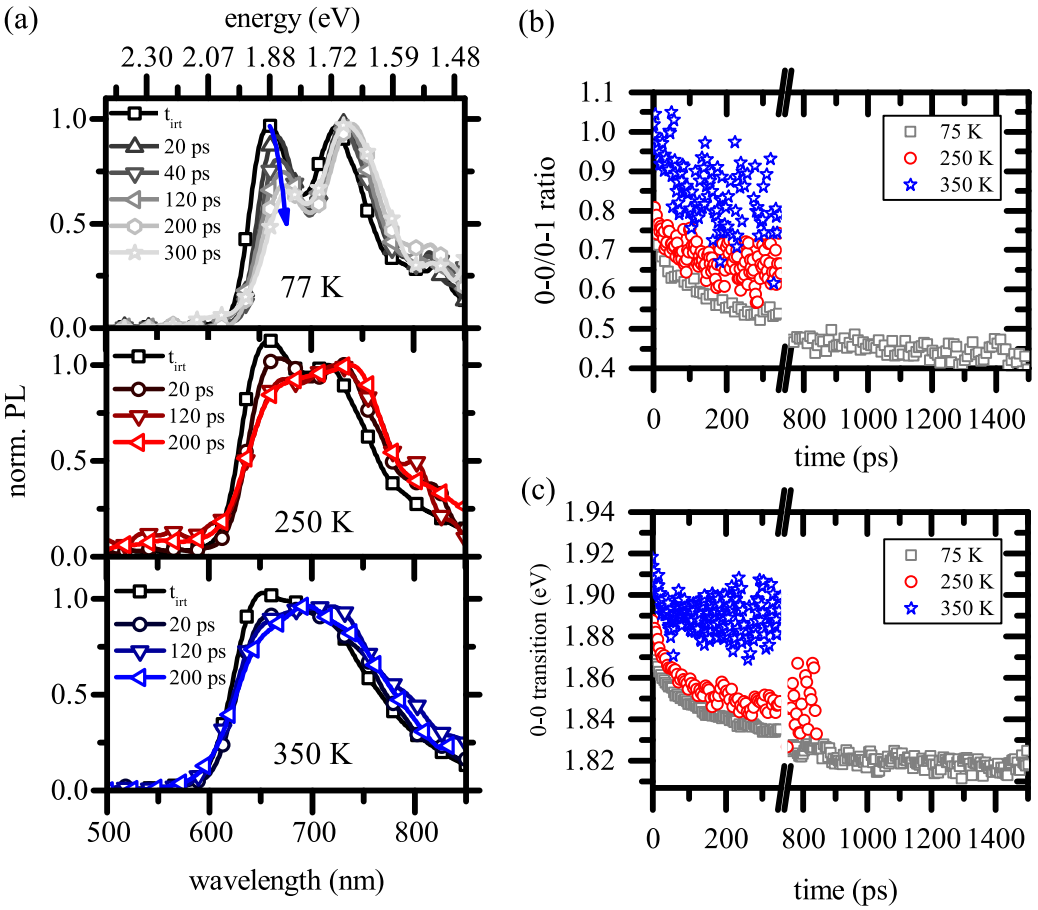

FIG. 4. (a) Time-resolved PL spectra of 50 nm rrP3HT films at selected temperatures (77, 250, and 350 K) representing the low-temperature (<200 K), intermediate-temperature (200–300 K), and high-temperature regimes (>350 K). (b) 0-0 to 0-1 transition ratio as a function of decay time. (c) Dynamic progression of the 0-0 transition. (b) and (c) are obtained from fits on streak camera spectra using Eq. (1).

transition can be interpreted as a probe for a dynamically changing local energetic environment of migrating excitons. In the following, we approximate the two migration regimes with a biexponential decay behavior. Doing so, we not only gain information about the activation temperature upon which excitons start to migrate via thermally activated hopping, but also we are able to quantify the impact of the occurrence of the high-energy emission peak on exciton lifetimes. For rrP3HT we extract $\tau_1 = 22 \pm 4$ ps and $\tau_2 = 141 \pm 19$ ps at room temperature (see Fig. 5). This is slightly shorter than what has been reported in the literature [16,18] and can be well explained by surface quenching occurring in thin films (see Sec. SIII of Supplemental Material [23]). Already for a 100 nm polymer film, the exciton lifetime is increased by a factor of more than 3. Our finding is consistent with earlier observations [25] and can be rationalized by slightly different film morphologies, surface polarization, or electron traps induced by oxygen at the film terminating surface [26,27]. In this work, we are not able to differentiate in between those; however, the fundamental physical mechanism of exciton migration stays qualitatively unaffected. This is justified by identical observations on decay dynamics using a different film thickness in the same temperature range (see Supplemental Material [23]). As shown in Fig. 5, exciton lifetimes are in rrP3HT temperature independent until 150 K. Upon a further temperature increase, extracted lifetimes reduce strongly. In general we observe that the fast decay component (τ_1) hardly depends on the energetic position at which it is evaluated, while the slow component (τ_2) is enhanced by roughly 20% at low temperatures, if the exciton lifetime is analyzed at the 0-1 transition instead of the 0-0 transition. This difference reduces around 200 K and vanishes in the intermediate temperature range between 200 and 300 K. Interestingly, the exciton lifetime is independent of the excitation wavelength (as shown in Fig. 5(b) or more detailed in the Supplemental Material [23]).

In the same fashion we have analyzed the fluorescence decay of rraP3HT. Also here the exciton lifetime is independent of temperature up to 150 K. In contrast to rrP3HT and the general expectation of thermally induced nonradiative quenching mechanisms, the exciton lifetime is strongly enhanced at 250 K. When analyzing the amplitude ratio of the two regimes it becomes obvious that the slow decay component is strongly enhanced (decrease in amplitude A_1) in this temperature range.

IV. DISCUSSION

A. Role of the glass transition temperature

Steady-state as well as time-resolved PL measurements reveal that excitons in rrP3HT indeed show an

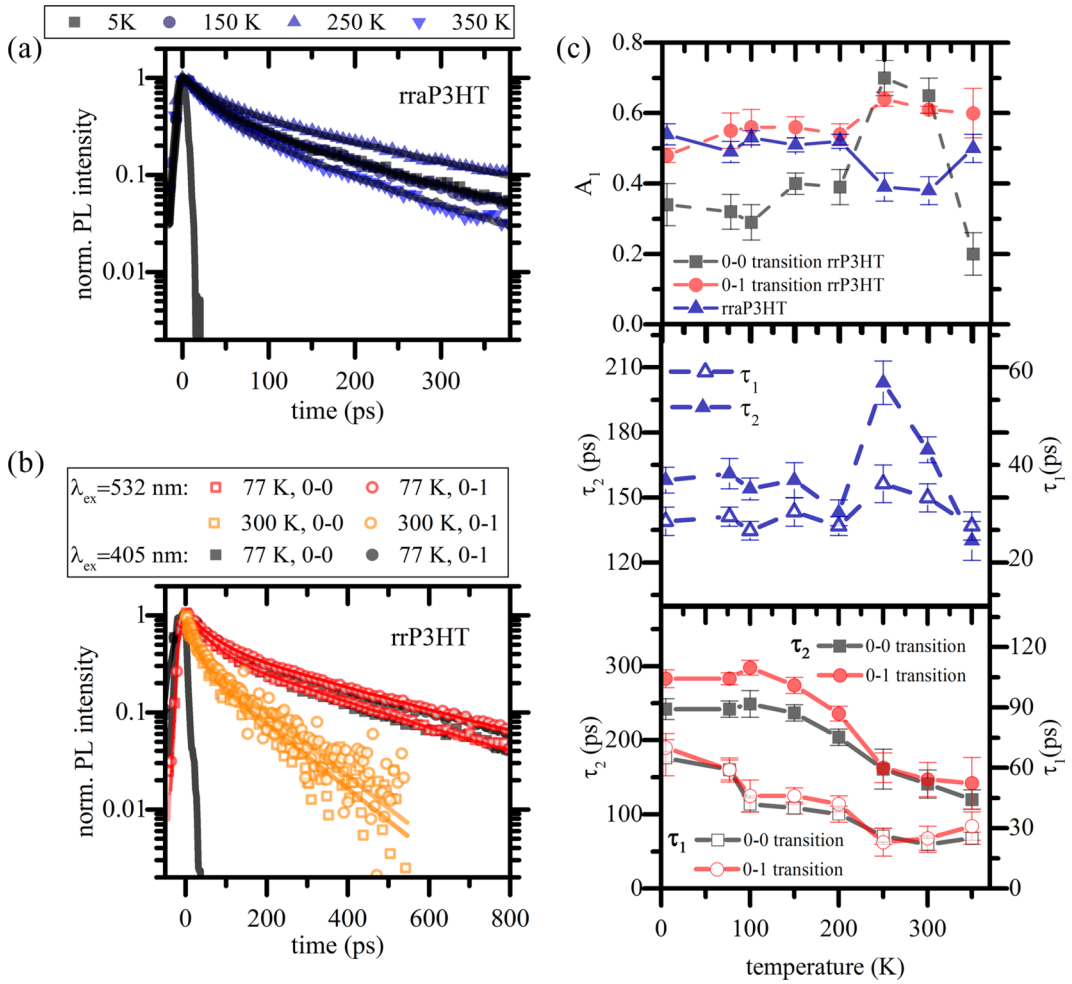

FIG. 5. Time-resolved PL decay dynamics taken of a 50 nm (a) rraP3HT film excited at 405 nm and (b) rrP3HT excited at 405 and 532 nm for various temperatures. The gray line shows the IRF, while solid lines on experimental data represent biexponential fits. (c) Fit results using an excitation wavelength of 405 nm; top: Amplitude A_1 of the first decay component; middle: decay times for rraP3HT; bottom: decay times for rrP3HT evaluated for the 0-0 and 0-1 transition. Lines are included as a guide for the eye and error bars represent the standard deviation obtained from fits.

excitation-energy-dependent emission spectrum in a certain temperature range. For temperatures between 250 and 300 K we observe an additional emission peak at energies larger than the optical gap for rrP3HT. For the same temperature range, excitons in rraP3HT exhibit longer lifetimes with enhanced radiative emission behavior. Interestingly, the high-energy emission in rrP3HT is virtually absent if mainly aggregated P3HT is excited at 532 nm for any temperature. Different from Chen *et al.* [19], we do not attribute hot-exciton emission to be responsible for this observation for the following reasons. First, even for excitation with 532 nm there is sufficient excess energy available for accessing such initially higher-lying electronic states from where emission should occur. Second, hot-exciton emission is a property that does not only occur in a narrow temperature range but rather increases at lower temperatures due to reduced nonradiative decay channels. Furthermore, Banerji *et al* [16]. could show that exciton relaxation happens on a time scale faster than 200 fs, during which more than 90% of the total Stokes shift and therefore localization takes place while the high-energy emission exhibits a ps lifetime as shown in this study. Instead, observations on rraP3HT are more conclusive and might better explain such an observation. In the same temperature range for which we observe a high-energy emission in rrP3HT, there is a strongly enhanced radiative emission in rraP3HT observed with longer exciton lifetimes. It is well known that P3HT exhibits a glass transition temperature T_g just below room temperature [28]. For this reason, we have analyzed the evolution of film thickness on temperature by means of ellipsometry. Below T_g, chain conformation is hampered and chain relaxation is prohibited [29]. Even for higher temperatures chain relaxation is confined in well-ordered aggregates and relaxation dynamics are limited. Therefore, the glass transition temperature is determined by the behavior of the fraction of amorphous polymer domains or mobile noninteracting chain segments [28,30]. At T_g, the thermal expansion coefficient changes due to a different elastic modulus of the glassy state and the rubbery state [29,31]. Since it is a second-order phase transition, volume and enthalpy change continuously [28]. As shown in the Supplemental Material [23], we determine T_g to occur around 250 K, a temperature that is close to those reported in the literature [28,32]. More interestingly,

however, it matches the lower edge of the temperature range in which we observe high-energy emission. It is important to note that T_g is not a physical constant, but rather depends on heating and cooling rates because the relaxation time is temperature dependent. Therefore, T_g is not limited to one specific temperature but can extend over a broader transition region if the measurement time and thus heating and cooling rates are much faster than the structural relaxation time. Glass transition temperature values in the literature may additionally vary due to influences of film thickness [33,34], molecular weight [35], free surfaces, interface interactions [29], and of course polydispersity [32]. Due to this fact, it is not surprising that the high-energy emission peak is not always observed in experiments that are typically performed at room temperature. The efficiency of exciton migration depends largely on intermolecular coupling, which is a function of temperature. Already, moderate temperatures can impact weak noncovalent forces by introducing low-frequency vibrations [36]. In addition, dynamic disorder, i.e., molecular and torsional motion around an equilibrium position, can influence the transfer integral between orbitals significantly [37]. For this reason, it is evident that the glass transition coincides with the temperature range in which we not only observe a high-energy emission in rrP3HT but also a strongly enhanced exciton lifetime for rraP3HT with an increased quantum yield. The latter two properties indicate that nonradiative decay losses are reduced at T_g, which can be rationalized by trapped excitons in decoupled and electronically isolated polymer chromophores. Due to negligible orbital overlap to neighboring energetic sites, these excitons are spatially localized and have to recombine radiatively while nonradiative channels and dissociation sites cannot be reached. Consequently, exciton diffusion from amorphous polymer domains into aggregates is suppressed and emission does not exclusively occur in highly ordered polymer domains anymore. This process is fundamentally different from hot-exciton emission since it is a diffusion-limited process and electronically localized excitons are recombining because of a disruption of orbital overlap. Also in steady-state PL spectra we found a significantly enhanced λ^2_{eff} suggesting stronger exciton localization [38]. Additionally, the 0-0/0-1 transition ratio is reduced, which can be explained either by improved H-aggregation or reduced interaction of excitons on the aggregated polymer to the amorphous matrix [11]. This observation, in combination with an increased PL intensity, however, further supports the conclusion of an electronic decoupling of aggregated and nonaggregated polymer domains.

B. Mechanism of exciton migration

Besides the high-energy emission peak, we have focused our work on seemingly different decay dynamics of the 0-0 transition compared to higher vibronic replicas. In general, the exciton lifetime is increasing by approximately a factor of 2 for temperatures below 150 K and determined exciton lifetimes at the 0-0 transition appear to be reduced. Such a dynamic decrease of the 0-0/0-1 transition ratio within the first tens of ps after excitation can result from a dynamic planarization of the polymer backbone or a migration process to lower energetic sites in the DOS [7,17]. We could show compelling evidence

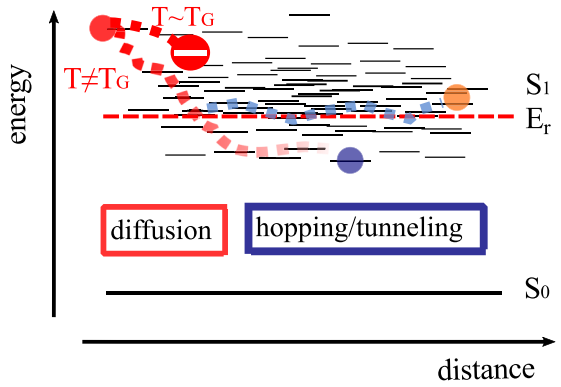

FIG. 6. Model of exciton diffusion, which is described by two regimes, namely exciton diffusion via energy transfer and exciton hopping to neighboring sites within a broad DOS. The latter process takes place at temperatures sufficient for thermal activation above the transport energy E_r (red dot) and is strongly limited at low temperatures (blue dot).

that these observations fit very well to the latter explanation (schematically shown in Fig. 6). After light absorption and exciton localization, excitons diffuse to lower energetic sites in an inhomogeneously broadened DOS. At low temperatures, excitons are trapped in the lowest energetic site they can reach, while thermally activated hopping occurs at temperatures above the mobility edge E_r. At low temperatures, downhill migration causes a dynamic redshift of approximately 60 meV. Above 150–200 K excitons get activated for hopping into higher-lying states such that the redshift is reduced to 20–25 meV at room temperature.

This interpretation is further supported by the occurrence of a PL anisotropy decay. As shown in the Supplemental Material [23], PL anisotropy decay takes place on a time scale similar to τ_1 in our samples. The fast decay component τ_1 therefore describes exciton diffusion via multistep energy transfer to lower energetic sites while τ_2 approximates the lifetime of excitons in its final state from where only diffusion via hopping is possible.

For determination of the width of the DOS it is necessary to evaluate the quantum efficiency η in more detail, which constitutes the ratio of the radiative decay rate (k_r) to the total decay rate:

$$\eta(T = 0\ K) = \frac{k_r}{k_r + k_{nr}}. \tag{3}$$

The dependence η on temperature is well described by the normalized PL intensity which is presented in Fig. 2, if we assume that the radiation profile is not changing significantly with temperature. Thermally activated hopping in the DOS enhances nonradiative contributions, leading to [38,39]

$$k_{nr}(T) = k^0_{nr} + k^T_{nr} e^{-(E_r/k_B T)}, \tag{4}$$

with a temperature-independent nonradiative decay rate k^0_{nr} and a temperature-dependent nonradiative decay rate constant k^T_{nr}. Normalization of η at 5 K and combining Eqs. (3) and (2)

leads to

$$\eta_{\mathrm{norm}}(T) = \frac{1}{1 + \frac{k_{nr}^{T}}{k_r + k_{nr}^{0}} e^{-(E_r/k_B T)}}. \quad (5)$$

This leaves the initial ratio of k_r vs k_{nr}^0 undefined, and relative changes of the quantum efficiency are exclusively attributed to thermally activated nonradiative recombination. A fit of the normalized temperature-dependent quantum efficiency with Eq. (5) let us determine the activation energy E_r to be 50 ± 8 meV in our films. In this analysis, we can only evaluate data on rrP3HT that is excited at 532 nm where influences of the glass transition temperature are virtually absent.

V. CONCLUSION

By means of temperature-dependent photoluminescence spectroscopy on P3HT, we observe (i) an increasing spectral redshift, (ii) a spectral peak narrowing, (iii) an increase of PL quantum yield, and (iv) a reduced 0-0/0-1 ratio at lower temperatures. These observations can be well explained within a diffusion-hopping transport model that has been successfully applied to a variety of different systems [7,20,21]. In this twofold exciton migration process nonradiative recombination of excitons is enhanced by a broad DOS [29,39–43]. During migration to lower-lying electronic states, dynamics of the 0-0 transitions appear to be affected by a change of the local environment of the excitation hosting chromophore.

Although there have been a great deal of investigations on the influence of the polymer glass transition temperature on mechanical characteristics, thermal stability, and its delamination behavior [28], little is known of its impact on electronic properties. In this study, we show compelling evidence that exciton diffusion from higher energetic amorphous polymer domains into aggregates can be hindered at T_g. This can be rationalized by a disturbed electronic coupling resulting in a high-energy emission peak in PL spectra of rrP3HT, i.e., localized excitons decay radiatively in less-ordered polymer domains.

Until now there are only few studies which show a strong dependence of charge-carrier generation on temperature and little is known about its influence on polaron formation. We demonstrate that electronic coupling between amorphous and aggregated domains can be very inefficient for excitons at the glass transition temperature, and electronic disorder dramatically decreases the mean exciton diffusion lengths. How the process of charge generation is influenced by the glass transition in detail remains an open question and demands further investigation.

In summary, P3HT can be well treated as a model system for investigations on exciton migration if we take its glass transition temperature into account. We could show that exciton migration is well explained within a diffusion-hopping model; however, at T_g electronic properties can change dramatically and energy-transfer processes are hindered. In this study, spectroscopic ellipsometry has been not only a suitable tool to uncover glass transition temperatures but also delivers temperature-induced changes in the material's dielectric properties. This is needed for an accurate investigation and modeling of exciton diffusion via photoluminescence spectroscopy.

ACKNOWLEDGMENT

We acknowledge funding from the German Federal Ministry of Education and Research (BMBF, MesoPIN project).

P.E. designed the experiments, fabricated the samples, and performed PL measurements. S.J. and A.G. performed additional PL measurements. D.P. measured low-temperature ellipsometry and performed its modeling. L.S.-M. and A.V.B. supervised the paper. All authors have contributed to the discussion and writing of this paper.

[1] S. Pröller, F. Liu, C. Zhu, C. Wang, T. P. Russell, A. Hexemer, P. Müller-Buschbaum, and E. M. Herzig, Adv. Energy Mater. **6**, 1501580 (2016).

[2] T. Pfadler, M. Coric, C. M. Palumbiny, A. C. Jakowetz, K.-P. Strunk, J. A. Dorman, P. Ehrenreich, C. Wang, A. Hexemer, R.-Q. Png, P. K. H. Ho, P. Müller-Buschbaum, J. Weickert, and L. Schmidt-Mende, ACS Nano **8**, 12397 (2014).

[3] T. Kim, J.-H. Kim, T. E. Kang, C. Lee, H. Kang, M. Shin, C. Wang, B. Ma, U. Jeong, T.-S. Kim, and B. J. Kim, Nat. Commun. **6**, 8547 (2015).

[4] G. Sauvé and R. Fernando, J. Phys. Chem. Lett. **6**, 3770 (2015).

[5] Y. Tamai, H. Ohkita, H. Benten, and S. Ito, J. Phys. Chem. Lett. **6**, 3417 (2015).

[6] D. E. Markov and P. W. M. Blom, Phys. Rev. B **74**, 085206 (2006).

[7] O. V. Mikhnenko, F. Cordella, A. B. Sieval, J. C. Hummelen, P. W. M. Blom, and M. A. Loi, J. Phys. Chem. B **112**, 11601 (2008).

[8] N. Banerji, J. Mater. Chem. C **1**, 3052 (2013).

[9] J. Clark, J.-F. Chang, F. C. Spano, R. H. Friend, and C. Silva, Appl. Phys. Lett. **94**, 163306 (2009).

[10] F. Paquin, H. Yamagata, N. J. Hestand, M. Sakowicz, N. Bérubé, M. Côté, L. X. Reynolds, S. A. Haque, N. Stingelin, F. C. Spano, and C. Silva, Phys. Rev. B **88**, 155202 (2013).

[11] F. C. Spano and C. Silva, Annu. Rev. Phys. Chem. **65**, 477 (2014).

[12] M. Brinkmann, J. Polym. Sci., Part B: Polym. Phys. **49**, 1218 (2011).

[13] P. Ehrenreich, S. T. Birkhold, E. Zimmermann, H. Hu, K.-D. Kim, J. Weickert, T. Pfadler, and L. Schmidt-Mende, Sci. Rep. **6**, 32434 (2016).

[14] C. Poelking, M. Tietze, C. Elschner, S. Olthof, D. Hertel, B. Baumeier, F. Wurthner, K. Meerholz, K. Leo, and D. Andrienko, Nat. Mater. **14**, 434 (2015).

[15] R. Tautz, E. Da Como, T. Limmer, J. Feldmann, H.-J. Egelhaaf, E. Von Hauff, V. Lemaur, D. Beljonne, S. Yilmaz, and I. Dumsch, Nat. Commun. **3**, 970 (2012).

[16] N. Banerji, S. Cowan, E. Vauthey, and A. J. Heeger, J. Phys. Chem. C **115**, 9726 (2011).

[17] P. Parkinson, C. Müller, N. Stingelin, M. B. Johnston, and L. M. Herz, J. Phys. Chem. Lett. **1**, 2788 (2010).
[18] F. Paquin, G. Latini, M. Sakowicz, P.-L. Karsenti, L. Wang, D. Beljonne, N. Stingelin, and C. Silva, Phys. Rev. Lett. **106**, 197401 (2011).
[19] K. Chen, A. J. Barker, M. E. Reish, K. C. Gordon, and J. M. Hodgkiss, J. Am. Chem. Soc. **135**, 18502 (2013).
[20] B. Mollay, U. Lemmer, R. Kersting, R. F. Mahrt, H. Kurz, H. F. Kauffmann, and H. Bässler, Phys. Rev. B **50**, 10769 (1994).
[21] L. M. Herz, C. Silva, A. C. Grimsdale, K. Müllen, and R. T. Phillips, Phys. Rev. B **70**, 165207 (2004).
[22] F. Laquai, Y.-S. Park, J.-J. Kim, and T. Basché, Macromol. Rapid Commun. **30**, 1203 (2009).
[23] See Supplemental Material at http://link.aps.org/supplemental/10.1103/PhysRevB.96.195204 for temperature-dependent PL spectra and polarization anisotropy measurements, as well as further fitting parameters. Low-temperature ellipsometer results are presented for a broader temperature range. The dependence of exciton lifetime on excitation energy, film thickness, and temperature is shown.
[24] J. Clark, C. Silva, R. H. Friend, and F. C. Spano, Phys. Rev. Lett. **98**, 206406 (2007).
[25] P. E. Shaw, A. Ruseckas, and I. D. W. Samuel, Adv. Mater. **20**, 3516 (2008).
[26] E. Mosconi, P. Salvatori, M. I. Saba, A. Mattoni, S. Bellani, F. Bruni, B. Santiago Gonzalez, M. R. Antognazza, S. Brovelli, G. Lanzani, H. Li, J.-L. Brédas, and F. De Angelis, ACS Energy Lett. **1**, 454 (2016).
[27] A. Sperlich, H. Kraus, C. Deibel, H. Blok, J. Schmidt, and V. Dyakonov, J. Phys. Chem. B **115**, 13513 (2011).
[28] C. Müller, Chem. Mater. **27**, 2740 (2015).
[29] H. Qin, D. Liu, and T. Wang, Adv. Mater. Interfaces **3**, 1600084 (2016).
[30] R. Remy, S. Wei, L. M. Campos, and M. E. Mackay, ACS Macro Lett. **4**, 1051 (2015).
[31] M. Campoy-Quiles, M. Sims, P. G. Etchegoin, and D. D. C. Bradley, Macromolecules **39**, 7673 (2006).
[32] F. Panzer, H. Bässler, and A. Köhler, J. Phys. Chem. Lett. **8**, 114 (2017).
[33] D. J. Pochan, E. K. Lin, S. K. Satija, and W.-l. Wu, Macromolecules **34**, 3041 (2001).
[34] T. Miyazaki, K. Nishida, and T. Kanaya, Phys. Rev. E **69**, 061803 (2004).
[35] L. Singh, P. J. Ludovice, and C. L. Henderson, Thin Solid Films **449**, 231 (2004).
[36] A. A. Bakulin, R. Lovrincic, X. Yu, O. Selig, H. J. Bakker, Y. L. A. Rezus, P. K. Nayak, A. Fonari, V. Coropceanu, J.-L. Bredas, and D. Cahen, Nat. Commun. **6**, 7880 (2015).
[37] J. Aragó and A. Troisi, Phys. Rev. Lett. **114**, 026402 (2015).
[38] I. Pelant and J. Valenta, *Luminescence Spectroscopy of Semiconductors* (Oxford University Press, Oxford, 2012).
[39] A. D. Platt, M. J. Kendrick, M. Loth, J. E. Anthony, and O. Ostroverkhova, Phys. Rev. B **84**, 235209 (2011).
[40] A. Y. Kobitski, R. Scholz, D. R. T. Zahn, and H. P. Wagner, Phys. Rev. B **68**, 155201 (2003).
[41] E. N. Bodunov, M. N. Berberan-Santos, and J. M. G. Martinho, Opt. Spectrosc. **91**, 694 (2001).
[42] A. Ruseckas, P. Wood, I. D. W. Samuel, G. R. Webster, W. J. Mitchell, P. L. Burn, and V. Sundström, Phys. Rev. B **72**, 115214 (2005).
[43] M. M.-L. Grage, Y. Zaushitsyn, A. Yartsev, M. Chachisvilis, V. Sundström, and T. Pullerits, Phys. Rev. B **67**, 205207 (2003).